ADVANCED FUNCTIONAL MATERIALS
www.afm-journal.de

A Core-Shell Nanoporous Pt-Cu Catalyst with Tunable Composition and High Catalytic Activity

*Xingbo Ge, Luyang Chen, Jianli Kang, Takeshi Fujita, Akihiko Hirata, Wei Zhang, Jianhua Jiang, and Mingwei Chen**

Composition-controlled fabrication of bimetallic catalysts is of significance in electrochemical energy conversion and storage. A novel nanoporous Pt-Cu bimetallic catalyst with a Pt skin and a Pt-Cu core, fabricated by electrochemically dealloying a bulk Pt-Cu binary alloy using a potential-controlled approach, is reported. The Pt/Cu ratio of the dealloyed nanoporous catalyst can be readily adjusted in a wide composition range by only controlling dealloying potential. The electro-catalytic performance of the nanoporous Pt-Cu catalyst shows evident dependence on Pt/Cu ratio although the surfaces of all the nanoporous catalysts are characterized to be covered by pure Pt. With optimal compositions, the dealloyed nanoporous Pt-Cu catalyst possesses enhanced electrocatalytic activities toward oxygen reduction reaction and formic acid oxidation in comparison with the commercial Pt/C catalyst.

1. Introduction

In the past two decades, proton exchange membrane fuel cells (PEMFC) catalyzed by platinum (Pt) have been extensively studied as a clean and effective energy technology, which is expected to be widely used in electric vehicles as a green energy source. However, the commercialization of this technology is mainly limited by the low natural abundance of Pt as well as the sluggish cathode oxygen reduction reaction (ORR), which results in serious efficiency loss and thus the demand of high Pt catalyst loading.[1] It has been found that alloying Pt with transition metals (such as Ni, Co, Rh, Fe, etc) can effectively decrease the Pt loading by enhancing both the catalytic activity and utilization of Pt.[2–15] Experimental and theoretical investigations have suggested that Pt-based bimetallic catalysts with a thin Pt-skin surface (even a Pt monolayer[16]) and a Pt-M (M = Ni, Co, Fe, etc.) core is an ideal structure for ORR because the modification of the d-band center of surface Pt atoms, caused by the underneath alloying effect, can enhance the catalysis.[17,18] Dealloying has been proved to be an effective approach for fabricating the core-shell structured bimetallic catalysts in the form of nanoparticles because the selective etching can remove the less-noble transition metals and naturally form a Pt passivated surface.[19–22]

Compared to extensive studies of Pt-Ni,[13–15] Pt-Co,[6,12] Pt-Fe[9] bimetallic catalysts, the Pt-Cu system has not been paid too much attention, particularly, for the application as an advanced catalyst for ORR. Machado et al. first studied the ORR activity of Pt with sub-monolayer Cu ad-atoms on surface. The Cu ad-atoms were found to show a strong inhibition on ORR of Pt in acid media.[23] Xiong et al. reported disordered Pt-Cu alloy catalysts for ORR, which showed much lower activity than Pt-Co and Pt-Ni bimetallic catalysts.[24,25] Tseng et al. first reported the enhanced catalytic activities of nanoparticulate Pt-Cu catalysts toward ORR.[26] Recently, Strasser and co-workers fabricated Pt-Cu core-shell nanoparticles by electrochemically dealloying nanoparticulate Pt-Cu made by an impregnation-reductive annealing method.[20] The enhanced ORR activity of the core-shell Pt-Cu nanoparticles has been demonstrated in both rotating disk electrodes and fuel cell experiments.[20,27] The activity enhancement has been attributed to the surface compressive strain from a pure Pt skin and a Pt-Cu alloy core.[21,28] The surface strain results in the downshift and broadening of the d-band of surface Pt and thus weakens the Pt-oxygen species bonding strength.[29] The electrocatalytic property is mainly dominated by the Pt/Cu ratio since the surface strain of the Pt skin is caused by the lattice mismatch with the underneath Pt-Cu alloy core.[30–33] In practice, a premeditated composition of bimetallic nanoparticulate catalysts is usually difficult to be precisely realized at the nanoscale. Therefore, developing a method that can easily control the composition of bimetallic catalysts is highly desired.

Dr. X. B. Ge, Dr. L. Y. Chen, Dr. J. L. Kang, Dr. T. Fujita, Dr. A. Hirata, Prof. M. W. Chen
WPI Advanced Institute for Materials Research
Tohoku University
Sendai 980-8577, Japan
E-mail: mwchen@wpi-aimr.tohoku.ac.jp
Prof. W. Zhang
School of Materials Science and Engineering
Dalian University of Technology
Dalian 116024, China
Dr. J. H. Jiang
School of Materials Science and Engineering
Shanghai Jiao Tong University
Shanghai 200030, P. R. China
Prof. M. W. Chen
State Key Laboratory of Metal Matrix Composites
School of Materials Science and Engineering
Shanghai Jiao Tong University, Shanghai 200030, P. R. China
Prof. M. W. Chen
CREST, JST, 4-1-8 Honcho Kawaguchi
Saitama 332-0012, Japan

DOI: 10.1002/adfm.201300114

Different from bottom-up wet chemical methods to synthesize bimetallic nanoparticulate catalysts, dealloying provides a unique approach to fabricate bimetallic catalysts by selectively etching one component from a ternary alloy. A number of nanoporous Pt-based bimetallic catalysts have been reported in the literature.[15,34–37] However, there are very few Pt-based ternary isomorphous systems available, limiting the development of Pt-based bimetallic catalysts with a uniform nanoporous structure and a widely tunable composition range. Moreover, since the dealloying process cannot completely remove the third elements from the ternary precursors, the residual elements, even in a trace amount, may significantly influence the catalytic performance of the catalysts.[38] In previous study, Pugh and co-workers have found that Pt-Cu alloys are an ideal system to fabricate nanoporous Pt by electrochemical dealloying.[39,40] In this study, we developed a potential-controlled dealloying method to fabricate a nanoporous Pt-Cu bimetallic catalyst with a wide range of Pt/Cu ratio by partially dissolving Cu from a binary $Pt_{15}Cu_{85}$ precursor in a controllable manner. The catalytic activity of the novel nanoporous catalyst shows significant composition dependence without the interference from third elements. With optimal Pt/Cu ratios, the dealloyed Pt-Cu catalyst presents very high catalytic activities toward ORR and formic acid oxidation.

2. Results and Discussion

2.1. The Fabrication of Pt-Cu Bimetallic Catalyst

Figure 1 a shows the linear sweep voltammetry (LSV) curve of $Pt_{15}Cu_{85}$ (at%) ribbons in 0.5 M H_2SO_4. Obvious dissolution of Cu occurs at ≈0.3 V and then the dealloying current sharply increases from ≈0.47 V vs. Ag/AgCl. The second rise of the dealloying current from ≈0.71 V vs. Ag/AgCl corresponds to the formation of Pt surface oxide. Since the Pt-skin type structure is more active for ORR,[18] in this study we selected the dealloying potentials lower than this value, i.e., 0.4, 0.5, 0.6, 0.7 V vs. Ag/AgCl, to dealloy the $Pt_{15}Cu_{85}$ alloy, aiming at the formation of a pure Pt-skin surface and a Pt-Cu core. Figure 1b is the typical dealloying curves of $Pt_{15}Cu_{85}$ at different potentials. At the first stage, the Cu dissolution is very fast due to the high content of Cu in the precursor. Upon Cu dissolving, exposed surface Pt atoms diffuse and assemble on the electrode surface to form a rough electrode/electrolyte interface. This process will expose more fresh surfaces thus accelerate the dealloying reaction, resulting in a gradually increased current. With the dissolution of the Cu atoms, the dealloying reaction gradually slows down due to the loss of the active Cu sites on the surface and thus the current decreases with time until the finish of the dealloying process. In general, a more positive applied potential means a larger drive force for Cu dissolution. Thus, the dealloying current is higher and the reaction can finish in a shorter time compared to a lower applied potential. For dealloying the $Pt_{15}Cu_{85}$ alloy with the same mass (about 7 mg) and initial surface area, it takes less than one hour to reach the threshold current of 5 μA at the applied potentials of 0.6 and 0.7 V, but more than 15 h at the applied potential of 0.4 V (Figure 1b: inset). The dealloyed Pt-Cu samples are very fragile, but still keep the ribbon shape and can be carefully handled as a bulk material.

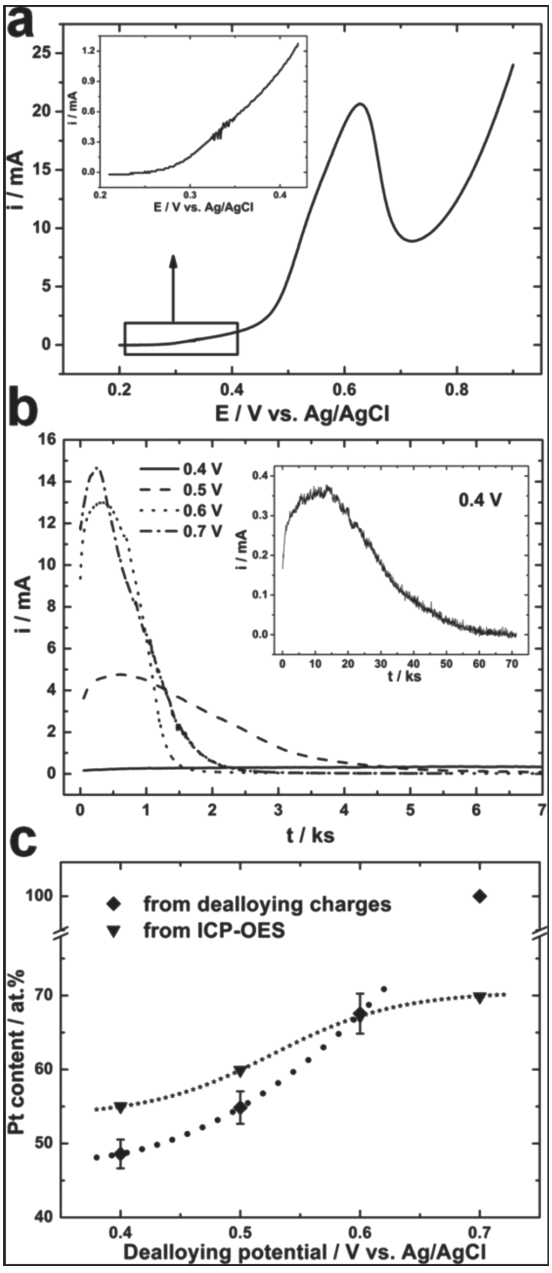

Figure 1. a) The LSV curve of the $Pt_{15}Cu_{85}$ alloy ribbons in 0.5 M H_2SO_4; b) Typical dealloying curves of $Pt_{15}Cu_{85}$ in 0.5 M H_2SO_4 at different potentials with the same mass and geometrical area; inset: the enlarged dealloying curve at 0.4 V. c) The compositions of the dealloyed Pt-Cu catalysts: estimated from the dealloying charges (diamonds) and determined using ICP-OES method (triangle).

Although the applied potentials are positive enough to dissolve Cu, complete dissolution of the Cu from the $Pt_{15}Cu_{85}$ precursor is unfeasible because the assembly of remained Pt atoms on the electrode surface will form a local passivation layer, which more or less prevent the further dissolution of underneath Cu. The mass of dissolved Cu can be estimated by Faraday's law:

$$m = \frac{MQ}{zF} \quad (1)$$

where M is the molar mass of Cu; Q is the total charge for Cu dissolution; z is the ionic charge; and F is the Faraday constant. If the current efficiency is 100%, the composition of the dealloyed Pt-Cu can be precisely calculated according to the dealloying charge since the initial mass of the Pt-Cu precursor alloy is known. As shown in Figure 1c, higher applied potentials give rise to higher Pt contents in the dealloyed samples. Dealloying at 0.4, 0.5, 0.6 and 0.7 V yields bimetallic Pt-Cu catalysts with chemical compositions of $Pt_{48}Cu_{52}$, $Pt_{55}Cu_{45}$, $Pt_{67}Cu_{33}$ and $Pt_{100}Cu_0$, respectively (Figure 1c), indicating that the potential-controlled dealloying approach can be utilized to fabricate bimetallic catalysts with tunable compositions. The irrationally high Pt concentration at 0.7 V is caused by the side reactions related to the formation of Pt-oxygen containing species and oxygen evolution on Pt surface.

The calculated potential dependence of the chemical compositions of the dealloyed nanoporous Pt-Cu is fairly consistent with the experimental measurements of the samples dealloyed at 0.4, 0.5 and 0.6 V. The chemical compositions of dealloyed samples were precisely measured by inductively coupled plasma optical emission spectrometry (ICP-OES). In the agreement with the charge calculations, higher dealloying potentials give rise to the higher Pt/Cu ratios. Dealloying at 0.4, 0.5, 0.6, 0.7 V vs. Ag/AgCl results in the nanoporous bimetallic Pt-Cu with Pt contents of 55, 60, 67.2, 69.8 at%, respectively (Figure 1c). By simply controlling the dealloying potentials, the composition of bimetallic Pt-Cu catalysts can be tailored in the range of ≈15 at%. It has been reported that the Pt-Cu bimetallic catalyst in this composition range (≈50–75 at% Pt) are highly active toward ORR.[21,32] Thus, this approach can be used for mass fabrication of highly-active Pt-Cu bimetallic catalysts for ORR. It is expected that a wider composition range can be achieve if we further adjust the dealloying potential window and the threshold current value. The obvious disparity between the ICP-OES measurement and charge calculation at the potential of 0.7 V is associated with reduced current efficiency and side reactions (e.g., the formation of Pt-oxygenated species and oxygen evolution) at the high applied potential.

2.2. The Structure Characterization of Pt-Cu Catalyst

The crystalline structure of the $Pt_{15}Cu_{85}$ precursor before and after dealloying was examined by X-ray diffraction (XRD) spectroscopy (**Figure 2**). The XRD pattern of the $Pt_{15}Cu_{85}$ ribbons exhibits a single-phase feature. The three sharp diffraction peaks located at 42.8, 49.8, and 73.0 can be indexed as the (111), (200), (220) planes of a face centered cubic (fcc) structure with a lattice constant closed to that of a $PtCu_3$ phase. The dealloyed samples also show three diffraction peaks located at 41.4, 48.1, and 70.4, synchronously shifting to the low angles, which can also be indexed as (111), (200), (220) planes of the fcc structure, respectively. The peak shift is mainly caused by the composition change associated with Cu dissolution by dealloying. Compared to those of the precursor $Pt_{15}Cu_{85}$ alloy, the peaks of the dealloyed Pt-Cu samples are much broader, which mainly results from the formation of nano-sized structure and heterogeneous surface strain. Besides above three peaks, no extra diffraction bands can be seen, suggesting the dealloyed Pt-Cu catalyst is still a uniform single-phase bimetallic alloy.

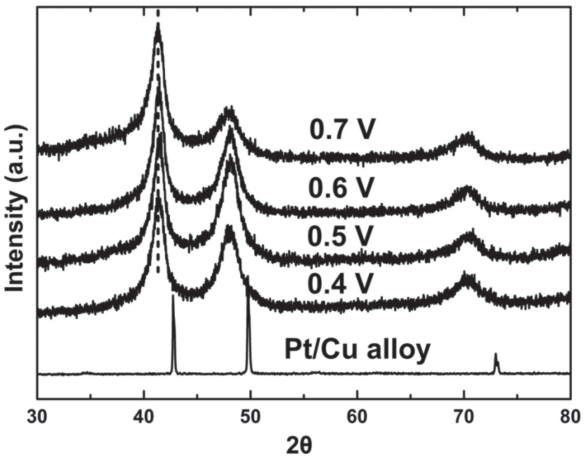

Figure 2. XRD patterns of $Pt_{15}Cu_{85}$ alloy and the dealloyed Pt-Cu samples.

The microstructure of the dealloyed Pt-Cu was investigated by scanning transmission electron microscopy (STEM) equipped with a high-angle annular dark field (HAADF) detector. **Figure 3** is the HAADF-STEM image showing the uniform nanoporous structure with the pore and ligament sizes of 3-5 nm. The relatively smaller pore size and porosity, compared to the Pt-Cu ligaments, are due to the overlapping of the 3D porous structure projecting to the 2D STEM image. This porous structure is very similar to that of other dealloyed Pt-based catalysts.[14,39] Dealloying Pt-based alloys often results in small pores and ligaments with a size less than 5 nm due to the low diffusivity of Pt at the alloy/electrolyte interface.[34,39] Meanwhile, the passivation Pt layer on the ligament surface prevents the interior Cu dissolution and thus considerable

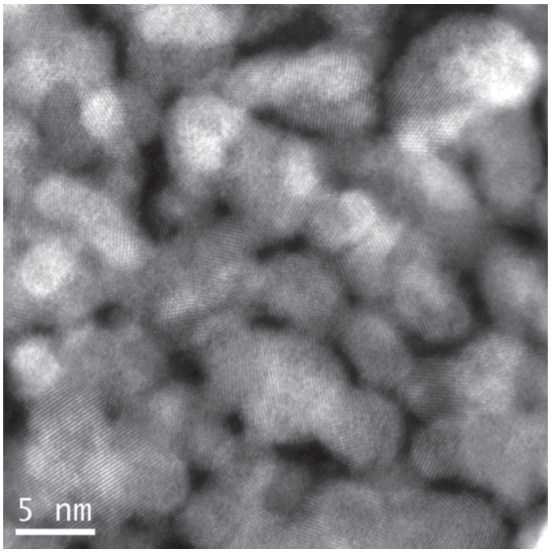

Figure 3. HAADF-STEM image of the dealloyed Pt-Cu at the potential of 0.6 V.

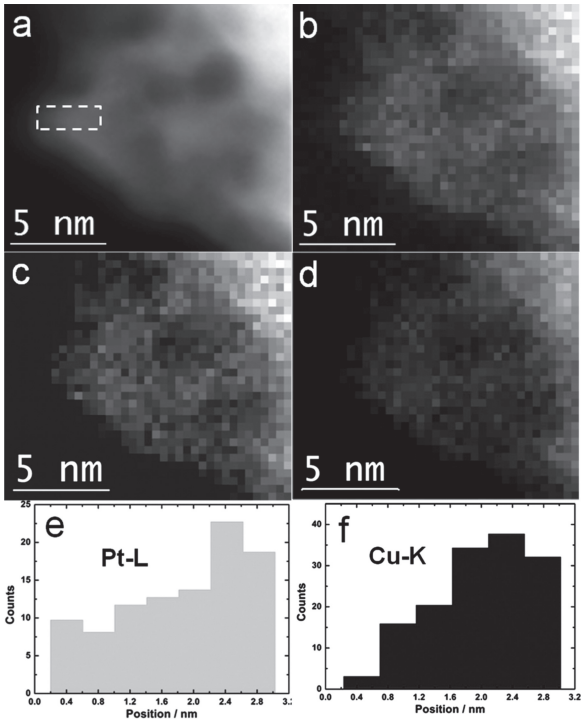

Figure 4. STEM image and EDS elemental maps of the dealloyed Pt-Cu ligament. a) HAADF-STEM image of the nanoporous structure; b) the mixed STEM-EDS elemental mappings of Pt-L & Cu-K; c) the elemental mapping of Pt-L; d) the elemental mapping of Cu-K. The composition intensity profile of e) Pt and f) Cu taken from the labeled region in (a).

Cu atoms can be remained in the final nanoporous structure. The distributions of Pt and Cu in the dealloyed samples were investigated by energy-dispersive X-ray spectroscopy (EDS) in a STEM mode. **Figure 4** shows the STEM-EDS elemental maps of a ligament in the 0.6 V dealloyed Pt-Cu sample. Both Pt and Cu can be detected, which appear to form a uniform alloy (Figure 4a–d). However, quantitative analysis shows that the Cu concentration in the surface and near surface (≈0.4 nm) region is much lower than that in the core, approaching to zero (Figure 4f), while considerable Pt atoms were detected at the surface region (Figure 4e), suggesting the formation of a thin Pt skin and a Pt-Cu alloy core. This core-shell structure has also been realized by dealloyed Pt-based nanoparticles. For example, the formation of the pure Pt shell with the thickness of ≈0.6 nm has been evidenced in dealloyed Pt-Cu nanoparticles.[21]

2.3. The Electrocatalytic Activities of Pt-Cu Catalyst

Figure 5a shows the typical cyclic voltammogram (CV) curves of a 0.6 V dealloyed Pt-Cu catalyst and commercial Pt/C catalyst in 0.1 M $HClO_4$ solution. The dealloyed Pt-Cu sample containing ≈67.2 at% Pt exhibits the voltammetric behaviors very similar to that of the Pt/C catalyst (pure Pt nanoparticles), i.e., hydrogen adsorption/desorption at 0.03–0.4 V, the electrochemical double layer at 0.4–0.6 V and the formation of Pt oxides and their reduction at 0.6–1.2 V vs. RHE. The absence of Cu signal in the CV curve of the dealloyed Pt-Cu unambiguously demonstrates the formation of a pure Pt surface after dealloying, consistent with the direct STEM-EDS observation. However, the chemical state of this Pt surface is apparently affected by the underlying Pt-Cu core. Compared with the commercial Pt/C catalyst, the reduction of the surface Pt oxides occurs at a much more positive potential on the 0.6 V dealloyed Pt-Cu catalyst, resulting in an obvious positive shift of the reduction peak. This positive shift suggests the weakening of Pt-oxygenated species, which was often observed from highly active ORR catalysts.[15,28] From the charge of hydrogen adsorption, the electrochemical active surface area (EASA) of the dealloyed Pt-Cu was determined to be ≈51 m^2/g Pt, comparable to that of the commercial Pt/C of ≈62 m^2/g.

ORR activities of the dealloyed Pt-Cu catalysts were evaluated by a rotating disk electrode at 1600 rpm. Figure 5b shows the polarization curves for ORR in a 0.1 M oxygen-saturated $HClO_4$ solution at room temperature. The polarization curve of Pt/C was also included for comparison. For both Pt/C and dealloyed Pt-Cu catalysts, two distinguishable potential regions can be observed, i.e., the mixed kinetic-diffusion controlled region from ≈0.75 to 1.0 V and the well-defined diffusion controlled region between 0.1 and ≈0.7 V with a diffusion limited current density of ≈6 mA/cm^2. As shown in the polarization curves, both the onset and half-wave potentials of the dealloyed Pt-Cu samples are more positive than that of Pt/C. For example, the 0.6 V dealloyed sample shows a half-wave potential of ≈0.89 V vs. RHE, more than 30 mV higher than that of Pt/C catalyst, suggesting the enhanced ORR activity at small overpotential. The kinetic current density (i_k) was calculated using the Koutecky–Levich (K–L) equation:

$$\frac{1}{i} = \frac{1}{i_k} + \frac{1}{i_d} \quad (2)$$

where i is the measured current, i_k is the kinetic current, and i_d is the measured limiting current. To accurately compare the intrinsic activities toward ORR, the i_k was normalized by the EASA as shown in Figure 5c. All the dealloyed Pt-Cu samples exhibit higher EASA specific kinetic activity than Pt/C. The 0.6 V dealloyed sample has the highest EASA specific activity at 0.9 V of ≈0.45 mA/cm^2, which is about three times higher than that of Pt/C measured at the same conditions. We notice that the Tafel curves of the dealloyed Pt-Cu samples (Figure 5c) intersect at high potentials. This most likely results from the structure variation of the dealloyed nanoporous Pt-Cu samples.[14,20] Since the nanopore size of the dealloyed Pt-Cu catalysts is only ≈3–5 nm, the mass transport can be significantly influenced by the sample thickness and hence the ORR activity. Erlebacher et al. have demonstrated that the ORR activity of nanoporous Pt-Ni decreases with the thickness of porous layers.[14]

Since the chemical composition is one of the fundamental factors determining the ORR activity of catalysts, we plotted the EASA specific activity versus the composition of the bimetallic Pt-Cu catalyst in Figure 5d. Although all the dealloyed Pt-Cu samples have a pure Pt surface, their ORR activities are strongly correlated with the Pt/Cu ratio. The $Pt_{55}Cu_{45}$ sample (dealloyed at 0.4 V) exhibits the lowest activity in the bimetallic Pt-Cu catalysts. Increasing the Pt content from ≈55 to 67 at% results in obvious improvement in the kinetic activity while

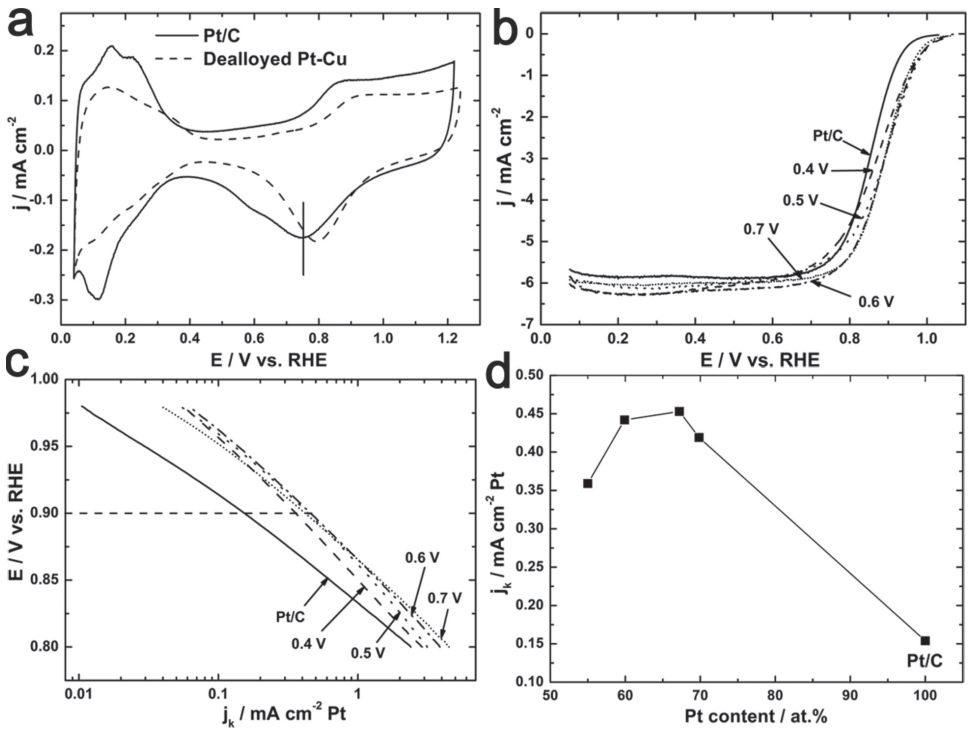

Figure 5. a) CV curves of the 0.6 V dealloyed nanoporous $Pt_{67.2}Cu_{32.8}$ and Pt/C catalysts in 0.1 M $HClO_4$. b) ORR polarization curves. c) EASA specific Tafel curves of dealloyed Pt-Cu and Pt/C in 0.1 M $HClO_4$, 1600 rpm, 5 mV/s, room temperature. d) The EASA specific activities at 0.9 V vs. Pt content (at%).

further increasing the Pt content to ≈70 at% leads to a slight decrease in the kinetic activity. Strasser and co-workers have showed that the activity of bimetallic Pt-Cu nanoparticles is very sensitive to the surface strain resulting from the lattice mismatch between the Pt-rich shell and the Pt-Cu core. Lower Pt content means higher Cu concentration in the core and larger compressive strain in the surface Pt skin.[21] The observed composition-dependent activity of the bimetallic nanoporous Pt-Cu catalysts shows a similar trend as that of the Pt-Cu nanoparticles, indicating both particulate and nanoporous Pt-Cu catalysts share the same mechanism although the latter has much more complex geometric morphology.

The electro-catalytic activities of the dealloyed Pt-Cu and commercial Pt/C catalysts toward formic acid oxidation were also investigated using the CV technique. For simplicity and easy comparison, we only show the forward scan curves of the EASA specific CVs here (**Figure 6**, the full scan data shown in Supporting Information Figure S1). All the catalysts show two current peaks at ≈0.58 and ≈0.92 V vs. RHE, which can be ascribed to the direct oxidation of formic acid via a dehydrogenation process and the oxidation of adsorbed CO species generated from the dehydration process, respectively.[41] While the dealloyed Pt-Cu samples exhibit nearly equal current density with Pt/C catalyst at the second peak except the $Pt_{55}Cu_{45}$ sample dealloyed at 0.4 V, they show obvious enhanced catalytic activity, compared with Pt/C, at the low potential peak. This suggests that the enhanced catalytic activity results from faster dehydrogenation process on the dealloyed nanoporous Pt-Cu surface, not inhibition of the formation of adsorbed CO. Isolated Pt atoms have been found to favorite direct dehydrogenation process.[42,43] This "ensemble effect" has also been observed from nanoporous catalysts by surface alloying[44] and depositing foreign atoms[45] to form discontinuous Pt surfaces. In our case, the core-shell Pt-Cu catalyst has a near pure Pt skin and, thus, the enhanced catalytic activity may not be completely from the discontinuous Pt surface. Instead, the composition depedence of the catalytic activity suggest that the underneath Pt-Cu alloys make the Pt skin more active for the oxidation of formic acid. Different from the strong composition dependence toward ORR, the dealloyed Pt-Cu samples present weak composition dependence for electro-oxidation of formic acid. With the decrease of the Pt content, the catalytic activity slight increases (Figure 6) and the sample with the lowest Pt loading ($Pt_{55}Cu_{45}$) possesses the highest catalytic performance in the whole potential range. This indicates that the large surface compression strain benefits the catalytic activity of Pt toward the formic electro-oxidation. Moreover, the high performance from low Pt loaded catalysts also have important implications for practical applications of the dealloyed bimetallic Pt-Cu catalysts in direct formic acid fuel cells with low catalyst costs.

3. Conclusion

By developing a potential-controlled dealloying approach, we have successfully fabricated a new type of nanoporous Pt-Cu bimetallic catalysts with a large EASA, comparable to 2–3 nm nanoparticles, and high catalytic activities toward ORR and

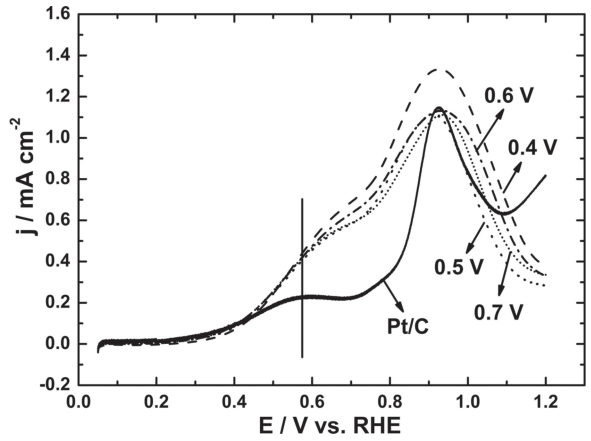

Figure 6. Formic acid electro-oxidation on dealloyed Pt-Cu and Pt/C at the scan rate of 50 mV/s.

formic electro-oxidation. The Pt/Cu ratio of the dealloyed Pt-Cu catalysts can be precisely adjusted in a wide composition range by tuning a single dealloying parameter of applied potentials. The dealloyed nanoporous Pt-Cu catalysts consist of a Pt-Cu alloy core and a pure Pt skin covering the entire internal surface of the nanoporous structure. The tunable Pt/Cu ratios in the core of the nanoporous structure provide an effective way to tailor the compressive strain in the surface Pt skin, which is believed to be the underlying mechanism for the enhanced catalytic activity of bimetallic catalysts. Consequently, the potential-controlled dealloying approach holds great promise for fabricating high-performance bimetallic catalysts toward energy-related reactions and applications.

4. Experimental Section

The Electrochemical Dealloying of Pt-Cu Alloys: All chemicals were used as received without any further purification. The binary $Pt_{15}Cu_{85}$ precursor was made by arc melting using pure Pt and Cu. The alloy was re-melted in a quartz tube and subsequently injected onto a rotating Cu wheel under Ar atmosphere to make $Pt_{15}Cu_{85}$ ribbons with thickness of ≈40 μm. The $Pt_{15}Cu_{85}$ alloy ribbons were annealed at 800 °C for 2 h in Ar atmosphere. The annealed ribbons (≈7 mg) were used as the work electrode and dealloyed in 0.5 M H_2SO_4 with an Ivium electrochemical workstation using chronoamperometry. For the potential-controlled dealloying, the dealloying potentials were chosen according to the LSV curve of the $Pt_{15}Cu_{85}$ ribbons in H_2SO_4. Ag/AgCl (Radiometer Analytical) and a Pt plate were used as the reference electrode and counter electrode, respectively.[46] The dealloying was assumed to finish when the current decreased to below a threshold value of 5 μA at various potentials. The dealloyed Pt-Cu samples were then transferred into deionized water (18.2 MΩ) and washed at least five times to remove the Cu ions and other residual chemicals. The as-prepared samples were dried in air for further characterization and electrochemical study.

The Structure and Composition Characterization of Pt-Cu Catalysts: The crystalline structure of the $Pt_{15}Cu_{85}$ alloy before and after dealloying was characterized by X-ray diffraction (XRD) using a Rigaku X-ray diffractometer with Cu Kα radiation (λ = 0.15405 nm). To determine the chemical compositions of the dealloyed Pt-Cu catalyst, the samples were dissolved in aqua regia and then analyzed by ICP-OES. Scanning electron microscope (SEM) (JEOL, JIB-4600F) was used to observe the morphology of the dealloyed Pt-Cu samples.

The microstructure and composition were also investigated using a transmission electron microscope (TEM) (JEOL JEM-2100F, 200 keV) equipped with double spherical aberration (Cs) correctors for both the probe-forming and image-forming objective lenses. Energy-dispersive X-ray spectroscopy (EDS) analysis was carried out using JEOL JED-2300T. High angle annular dark field (HAADF) images were acquired using an annular-type scanning TEM (STEM) detector.

Electrochemical Measurements: All electrochemical measurements were performed on an electrochemical workstation (Ivium Technology) in a standard three-electrode cell. Same as the dealloying configuration, Ag/AgCl and a Pt plate were selected as the reference electrode and counter electrode, respectively. For comparison, some potential values used in the text were reported versus the reversible hydrogen electrode (RHE). The electrochemical experiments were carried out at room temperature (≈20 °C). All the electrodes were first cycled in deoxygenated 0.1 M $HClO_4$ between 0.05 and 1.2 V for 40 cycles at 100 mV/s. Then the CV curves were taken at 50 mV/s. The EASA of the catalysts was determined by integrating the hydrogen adsorption charge using a conversion factor of 210 μC/cm^2. ORR experiments were carried out on a rotating disk electrode system (Pine Inst.) in an O_2 saturated 0.1 M $HClO_4$ solution. The ORR activities were evaluated by LSV at 5 mV/s. Formic acid oxidation was performed in a mixed solution of 0.1 M $HClO_4$ and 0.2 M HCOOH using a CV technique at 50 mV/s. The electrolyte was purged with high pure N_2 for 30 min prior to the measurement.

Supporting Information

Supporting Information is available from the Wiley Online Library or from the author.

Acknowledgements

This work was sponsored by JST-CREST "Phase Interface Science for Highly Efficient Energy Utilization", JST, Japan; and World Premier International (WPI) Research Center Initiative for Atoms, Molecules and Materials, MEXT, Japan. T.F. was supported by JST-PRESTO.

Received: January 10, 2013
Revised: February 7, 2013
Published online: March 26, 2013

[1] H. A. Gasteiger, S. S. Kocha, B. Sompalli, F. T. Wagner, *Appl. Catal. B: Environ.* **2005**, *56*, 9.
[2] T. Toda, H. Igarashi, H. Uchida, M. Watanabe, *J. Electrochem. Soc.* **1999**, *146*, 3750.
[3] V. R. Stamenkovic, B. S. Mun, K. J. J. Mayrhofer, P. N. Ross, N. M. Markovic, *J. Am. Chem. Soc.* **2006**, *128*, 8813.
[4] V. R. Stamenkovic, T. J. Schmidt, P. N. Ross, N. M. Markovic, *J. Phys. Chem. B* **2002**, *106*, 11970.
[5] N. Wakabayashi, M. Takeichi, H. Uchida, M. Watanabe, *J. Phys. Chem. B* **2005**, *109*, 5836.
[6] S. Chen, P. J. Ferreira, W. Sheng, N. Yabuuchi, L. F. Allard, Y. Shao-Horn, *J. Am. Chem. Soc.* **2008**, *130*, 13818.
[7] V. A. Paulus, A Wokaun, G. G. Scherer, T. J. Schmidt, V. R. Stamenkovic, V. Radmilovic, N. M. Markovic, P. N. Ross, *J. Phys. Chem. B* **2002**, *106*, 4181.
[8] J. X. Wang, H. Inada, L. Wu, Y. Zhu, Y. Choi, P. Liu, W. P. Zhou, R. R. Adzic, *J. Am. Chem. Soc.* **2009**, *131*, 17298.
[9] J. I. Shui, C. Chen, J. C. M. Li, *Adv. Funct. Mater.* **2011**, *21*, 3357.
[10] B. Lim, M. Jiang, P. H. C. Camargo, E. C. Cho, J. Tao, X. Lu, Y. Zhu, Y. Xia, *Science* **2009**, *324*, 1302.
[11] Z. Peng, H. Yang, *J. Am. Chem. Soc.* **2009**, *131*, 7542.
[12] Y. Zhang, M. Janyasupab, C-W. Liu, X. Li, J. Xu, C-C. Liu, *Adv. Funct. Mater.* **2012**, *22*, 3570

[13] V. R. Stamenkovic, B. Fowler, B. S. Mun, G. Wang, P. N. Ross, C. A. Lucas, N. M. Markovic, *Science* **2007**, *315*, 493.
[14] J. Snyder, T. Fujita, M. W. Chen, J. Erlebacher, *Nat. Mater.* **2010**, *9*, 904.
[15] R. Wang, C. Xu, X. Bi, Y. Ding, *Energy Environ. Sci.* **2012**, *5*, 5281.
[16] M. B. Vukmirovic, J. Zhang, K. Sasaki, A. U. Nilekar, F. Uribe, M. Mavrikakis, R. R. Adzic, *Electrochim. Acta* **2007**, *52*, 2257.
[17] V. R. Stamenkovic, B. S. Mun, K. J. J. Mayrhofer, P. N. Ross, N. M. Markovic, J. Rossmeisl, J. K. Norskov, *Angew. Chem. Int. Ed.* **2006**, *45*, 2897.
[18] V. R. Stamenkovic, B. S. Mun, M. Arenz, K. J. J. Mayrhofer, C. A. Lucas, G. Wang, P. N. Ross, N. M. Markovic, *Nat. Mater.* **2007**, *6*, 241.
[19] C. Wang, M. Chi, D. Li, D. Strmcnik, D. Vliet, G. Wang, V. Komanicky, K. C. Chang, A. P. Paulikas, D. Tripkovic, J. Pearson, K. L. More, N. M. Markovic, V. R. Stamenkovic, *J. Am. Chem. Soc.* **2011**, *133*, 14396.
[20] S. Koh, P. Strasser, *J. Am. Chem. Soc.* **2007**, *129*, 12624.
[21] P. Strasser, S. Koh, T. Anniyev, J. Greeley, K. More, C. F. Yu, Z. C. Liu, S. Kaya, D. Nordlund, H. Ogasawara, M. F. Toney, A. Nilsson, *Nat. Chem.* **2010**, *2*, 454.
[22] J. Snyder, I. McCue, K. Livi, J. Erlebacher, *J. Am. Chem. Soc.* **2012**, *134*, 8633.
[23] S. A. S. Machado, A. A. Tanaka, E. R. Gonzalez, *Electrochim. Acta* **1991**, *36*, 1325.
[24] L. Xiong, A. Manthiram, *J. Mater. Chem.* **2004**, *14*, 1454.
[25] L. Xiong, A. Manthiram, *J. Electrochem. Soc.* **2005**, *152*, A697.
[26] C. J. Tseng, S. T. Lo, S. C. Lo, P. P. Chu, *Mater. Chem. Phys.* **2006**, *100*, 385.
[27] P. Mani, R. S. Srivastava, P. Strasser, *J. Phys. Chem. C* **2008**, *112*, 2770.
[28] R. Yang, J. Leisch, P. Strasser, M. F. Toney, *Chem. Mater.* **2010**, *22*, 4712.
[29] I. E. L. Stephens, A. S. Bondarenko, F. J. Perez-Alonso, F. G. Calle-Vallejo, L. Bech, T. P. Johansson, A. K. Jepsen, R. Frydendal, B. P. Knudsen, J. Rossmeisl, I. Chorkendorff, *J. Am. Chem. Soc.* **2011**, *133*, 5485.
[30] M. Oezaslan, P. Strasser, *J. Power Sources* **2011**, *196*, 5240.
[31] R. Yang, P. Strasser, M. F. Toney, *J. Phys. Chem. C* **2011**, *115*, 9074.
[32] S. Koh, N. Hahn, C. Yu, P. Strasser, *ECS Trans.* **2008**, *16*, 1093.
[33] D. Xu, S. Bliznakov, Z. Liu, J. Fang, N. Dimitrov, *Angew. Chem. Int. Ed.* **2010**, *49*, 1282.
[34] C. Xu, R. Wang, M. Chen, Y. Zhang, Y. Ding, *Phys. Chem. Chem. Phys.* **2010**, *12*, 239
[35] H. J. Jin, X. L. Wang, S. Parida, K. Wang, M. Seo, J. Weissmuller, *Nano Lett.* **2010**, *10*, 187.
[36] J. Snyder, P. Asanithi, A. B. Dalton, J. Erlebacher, *Adv. Mater.* **2008**, *20*, 4883.
[37] C. Xu, L. Wang, X. Mu, Y. Ding, *Langmuir* **2010**, *26*, 7437.
[38] T. Fujita, P. Guan, K. McKenna, X. Lang, A. Hirata, L. Zhang, T. Tokunaga, S. Arai, Y. Yamamoto, N. Tanaka, Y. Ishikawa, N. Asao, Y. Yamamoto, J. Erlebacher, M. Chen, *Nat. Mater.* **2012**, *11*, 775.
[39] D. V. Pugh, A. Dursun, S. G. Corcoran, *J. Mater. Res.* **2003**, *18*, 216.
[40] D. V. Pugh, A. Dursun, S. G. Corcoran, *J. Electrochem. Soc.* **2005**, *152*, B455.
[41] H. Okamoto, W. Kon, Y. Mukouyama, *J. Phys. Chem. B* **2005**, *109*, 15659.
[42] S. C. Chang, Y. Ho, M. J. Weaver, *Surf. Sci.* **1992**, *265*, 81.
[43] S. Park, Y. Xie, M. J. Weaver, *Langmuir* **2002**, *18*, 5792.
[44] X. Ge, X. Yan, R. Wang, F. Tian, Y. Ding, *J. Phys. Chem. C* **2009**, *113*, 7379.
[45] R. Wang, C. Wang, W. B. Cai, Y. Ding, *Adv. Mater.* **2010**, *22*, 1845.
[46] L. Y. Chen, H. Guo, T. Fujita, A. Hirata, W. Zhang, A. Inoue, M. W. Chen, *Adv. Funct. Mater.* **2011**, *21*, 4364.